Title

A Small-molecule Screen Yields Idiotype-specific Blockers of Neuromyelitis Optica Immunoglobulin G Binding to Aquaporin-4*

Journal

Journal of Biological Chemistry, 287(44)

ISSN

0021-9258

Authors

Phuan, Puay-Wah
Anderson, Marc O
Tradtrantip, Lukmanee
et al.

Publication Date

2012-10-01

DOI

10.1074/jbc.m112.408716

THE JOURNAL OF BIOLOGICAL CHEMISTRY VOL. 287, NO. 44, pp. 36837–36844, October 26, 2012

A Small-molecule Screen Yields Idiotype-specific Blockers of Neuromyelitis Optica Immunoglobulin G Binding to Aquaporin-4*

Received for publication, August 7, 2012 Published, JBC Papers in Press, September 18, 2012, DOI 10.1074/jbc.M112.408716

Puay-Wah Phuan[‡], Marc O. Anderson[§], Lukmanee Tradtrantip[‡], Hua Zhang[‡], Joseph Tan[‡], Chiwah Lam[¶], Jeffrey L. Bennett[¶], and A. S. Verkman[‡1]

From the [‡]Departments of Medicine and Physiology, University of California, San Francisco, California 94143-0521, the [§]Department of Chemistry and Biochemistry, San Francisco State University, San Francisco, California 94132-4136, and the [¶]Departments of Neurology and Ophthalmology, University of Colorado Denver, Aurora, Colorado 80045

Background: A high-throughput cytotoxicity-based screen was developed to identify small-molecule inhibitors of NMO-IgG-AQP4 binding.
Results: Pyrano[2,3-*c*]pyrazoles were identified as inhibitors and were shown to bind directly to the NMO monoclonal antibody used for screening but did not interfere with other NMO-IgGs that bound to AQP4.
Conclusion: Pyrano[2,3-*c*]pyrazoles are idiotype-specific to the NMO recombinant monoclonal antibody used for screening.
Significance: Our results establish a proof of concept for an antibody-targeted small-molecule blocker strategy to prevent specific antibody-antigen binding.

Neuromyelitis optica (NMO) is an inflammatory demyelinating disease of the central nervous system caused by binding of anti-aquaporin-4 (AQP4) autoantibodies (NMO-IgG) to AQP4 on astrocytes. A screen was developed to identify inhibitors of NMO-IgG-dependent, complement-dependent cytotoxicity. Screening of 50,000 synthetic small molecules was done using CHO cells expressing human AQP4 and a human NMO recombinant monoclonal antibody (rAb-53). The screen yielded pyrano[2,3-*c*]pyrazoles that blocked rAb-53 binding to AQP4 and prevented cytotoxicity in cell culture and spinal cord slice models of NMO. Structure-activity analysis of 82 analogs yielded a blocker with $IC_{50} \sim 6\ \mu M$. Analysis of the blocker mechanism indicated idiotype specificity, as (i) pyrano[2,3-*c*]pyrazoles did not prevent AQP4 binding or cytotoxicity of other NMO-IgGs, and (ii) surface plasmon resonance showed specific rAb-53 binding. Antibody structure modeling and docking suggested a putative binding site near the complementarity-determining regions. Small molecules with idiotype-specific antibody targeting may be useful as research tools and therapeutics.

Antibodies are widely used as tools in cell biology and as therapeutics and are implicated in the pathogenesis of various autoimmune diseases (1–3). The variable region of the Fab portion of an antibody confers idiotype specificity. A typical maneuver to reduce antibody-target interaction is the addition of excess bystander target or target mimic to reduce the concentration of unbound antibody. Small molecules that bind to antibodies with idiotype specificity could provide a potential alternative approach to block antibody binding. Small-molecule blockers could be useful as research tools in cell biology, as controls for antibody specificity, and as therapeutics for autoimmune diseases or tumors associated with clonally expanded cell populations or for neutralization of excess administered monoclonal antibodies.

We recently introduced candidate therapeutics for the autoimmune disease neuromyelitis optica (NMO),[2] in which inflammatory demyelinating lesions of the central nervous system are caused by binding of serum autoantibodies (NMO-IgG) to aquaporin-4 (AQP4) (4–6). AQP4 is a plasma membrane water channel expressed on astrocytes (7), which, when targeted by NMO-IgG, causes complement-dependent cytotoxicity and inflammation, resulting in secondary damage to oligodendrocytes and neurons (8–11). We developed a blocker antibody (aquaporumab) approach in which a high-affinity anti-AQP4 monoclonal antibody was mutated to prevent its cytotoxicity effector functions (12). In an alternative approach, a small-molecule screen based on NMO-IgG binding to AQP4-expressing cells yielded blockers that targeted the extracellular surface of AQP4 and reduced NMO-IgG binding (13).

To identify more potent small-molecule blockers for NMO therapy, here we implemented a cytotoxicity-based screen of NMO-IgG binding to AQP4. Interestingly, the screen yielded several idiotype-specific small-molecule blockers, one of which was further characterized.

EXPERIMENTAL PROCEDURES

Cell Lines and Antibodies—CHO cells expressing human M23-AQP4 were generated by stable transfection as described

* This work was supported, in whole or in part, by National Institutes of Health Grants EY13574, EB00415, DK35124, HL73856, DK86125, and DK72517 (to A. S. V.). This work was also supported by grants from the Guthy-Jackson Charitable Foundation (to A. S. V. and J. L. B.) and Grant RG4320 from the National Multiple Sclerosis Society (to J. L. B.).

[1] To whom correspondence should be addressed: University of California, 1246 Health Sciences East Tower, University of California, San Francisco, CA 94143-0521. Tel.: 415-476-8530; Fax: 415-665-3847; E-mail: alan.verkman@ucsf.edu.

[2] The abbreviations used are: NMO, neuromyelitis optica; AQP4, aquaporin-4; rAb, recombinant antibody; HBSS, Hanks' balanced salt solution; LDH, lactate dehydrogenase; SPR, surface plasmon resonance; GFAP, glial fibrillary acidic protein; CDR, complementarity-determining region.

(14). CHO cells were cultured in Ham's F-12 nutrient mixture supplemented with 10% fetal bovine serum, 100 units/ml penicillin, and 100 μg/ml streptomycin. Geneticin (200 μg/ml) was used as a selection marker. Cells were grown at 37 °C in 5% CO_2 and 95% air. NMO recombinant monoclonal antibodies (NMO-rAbs) were generated from clonally expanded plasmablasts from cerebrospinal fluid of NMO patients and purified as described (15). A non-NMO-rAb (rAb-2B4) against measles virus nucleocapsid protein was used as a control isotype-matched antibody. NMO serum was obtained from NMO-IgG-seropositive individuals who met the revised diagnostic criteria for clinical disease (16). Non-NMO serum was used as a control. For some studies, IgG was purified from NMO or control serum and concentrated using a Melon gel IgG purification kit (Thermo Fisher Scientific, Rockford, IL) and Amicon Ultra centrifugal filter units (Millipore, Billerica, MA).

High-throughput Screening—Screening of 50,000 synthetic small molecules was performed (ChemDiv, San Diego, CA). Screening was carried out using an integrated apparatus (Beckman Coulter, Fullerton, CA) consisting of a CO_2 incubator, plate washer, Biomek FX liquid handling station, and plate readers. M23-AQP4-expressing CHO cells were plated onto 96-well Costar microplates (Corning, Corning, NY) at 15,000 cells/well and grown at 37 °C and 5% CO_2 for 18–24 h. Eighty wells contained test compounds, and the first and last columns of each plate were used for negative (no test compound) and positive (human complement only) controls. For screening, cells were washed with Hanks' balanced salt solution (HBSS; without phenol red), leaving 45 μl of HBSS. Test compounds were added (0.5 μl of 2.5 mM Me_2SO solution) to each well at a final concentration of 25 μM and incubated for 10 min at room temperature. A premixed solution (5 μl) of NMO-IgG (rAb-53, 30 μg/ml) and 20% pooled normal human complement serum (Innovative Research, Novi, MI) was added to each well to give a final volume of 50 μl. After 1 h of incubation at room temperature, lactate dehydrogenase (LDH) release was measured by addition of 50 μl of CytoTox-ONE homogeneous membrane integrity assay solution (Promega, Madison, WI) according to the manufacturer's protocol. LDH concentration was assayed from resorufin fluorescence (excitation/emission at 560/590 nm). Percentage cytotoxicity was computed as ((compound − negative control)/(positive control − negative control)) × 100. For live/dead cell staining, cells were washed with HBSS and then incubated with 1 μM calcein-AM (live cells, green fluorescence) and 2 μM ethidium homodimer-1 (dead cells, red fluorescence) (Invitrogen) in PBS for 15 min prior to imaging.

NMO-IgG Binding—M23-AQP4-expressing CHO cells were plated onto 96-well microplates and grown for 18–24 h to confluence. Cells were washed twice with PBS and blocked with 1% BSA in PBS for 30 min. After removal of the blocking solution, test compounds in PBS (90 μl, 1% Me_2SO) were added and incubated for 30 min at room temperature. A premixed solution (10 μl) of NMO-rAb (10 μg/ml) and HRP-labeled goat anti-human IgG secondary antibody (1:50 dilution; Invitrogen) was then added. Following 1 h of incubation at room temperature, cells were washed three times with PBS containing 0.05% Tween 20, and HRP activity was assayed by addition of 50 μl of Amplex Red substrate (100 μM; Sigma) and 2 mM H_2O_2 as described (12). Fluorescence was measured after 10 min (excitation/emission at 540/590 nm).

Immunostaining—Cells were grown on glass coverslips for 24 h. Cells were then washed with PBS and incubated for 30 min in live cell blocking buffer (PBS containing 6 mM glucose, 1 mM sodium pyruvate, and 1% BSA). Cells were incubated with compound or control (Me_2SO) for 30 min and then for 60 min with NMO-rAb at a final concentration of 1 μg/ml in blocking buffer. Cells were rinsed in PBS, fixed in 4% paraformaldehyde for 15 min, and permeabilized with 0.1% Triton X-100. Cells were incubated for 60 min with 0.4 μg/ml C terminus-specific rabbit anti-AQP4 polyclonal antibody (H-80; Santa Cruz Biotechnology, Santa Cruz, CA) and then for 30 min with 4 μg/ml Alexa Fluor 488-conjugated goat anti-human IgG and 4 μg/ml Alexa Fluor 555-conjugated goat anti-rabbit IgG (Invitrogen) in blocking buffer as described (17). Red and green fluorescence was imaged on a Nikon Eclipse TE2000S inverted epifluorescence microscope.

Surface Plasmon Resonance—Surface plasmon resonance (SPR) measurements were done on a Biacore T100 instrument (GE Healthcare). NMO-rAbs and control antibody (rAb-2B4) were diluted with 10 mM sodium acetate buffer (pH 5.5) to 20 μg/ml and immobilized onto the surface of a carboxymethylate-functionalized CM5 sensor chip (GE Healthcare) using standard carbodiimide coupling. Unreacted surface was blocked by injecting 1 M ethanolamine HCl. The reference control flow cell was coupled with 1 M ethanolamine HCl only. Binding was measured at 25 °C using pH 7.4 HEPES-buffered saline containing 5% Me_2SO as running buffer at a flow rate of 30 μl/min. Small molecules in identical buffer were injected for 25 s over a sensor chip at the same flow rate. Sensorgrams were corrected by subtraction of responses of the unloaded reference flow cell. Equilibrium constants for small molecule-antibody binding were determined using a 1:1 Langmuir binding affinity model.

Ex Vivo Spinal Cord Slice Model of NMO—Wild-type and AQP4-null mice on a CD1 genetic background were used as generated and characterized previously (18). Transverse slices of cervical spinal cord with a thickness of 300 μm were cut from postnatal day 7 pups using a vibratome and placed in ice-cold HBSS (pH 7.2) as described (19). Slices were placed on transparent membrane inserts (Millicell-CM (0.4-μm pores, 30-mm diameter), Millipore) in 6-well plates containing 1 ml of culture medium, with a thin film of culture medium covering the slices. Slices were cultured in 5% CO_2 at 37 °C for 7 days in 50% minimum Eagle's medium, 25% HBSS, 25% horse serum, 1% penicillin/streptomycin, 0.65% glucose, and 25 mM HEPES. On day 7, slices were incubated with blocker for 1 h, and then rAb-53 (10 μg/ml) and human complement (5%) were added to the culture medium on both sides of the slices. Slices were cultured for an additional 24 h and immunostained for AQP4 and glial fibrillary acidic protein (GFAP). Sections were scored as follows: 0, intact slice with normal GFAP and AQP4 staining; 1, mild astrocyte swelling and/or reduced AQP4 staining; 2, at least one lesion with loss of GFAP and AQP4 staining; 3, multiple lesions affecting >30% of the slice area; and 4, lesions affecting >80% of the slice area.

Antibody Structure Modeling and Molecular Docking—The Web-based antibody homology modeling tool PIGS (prediction

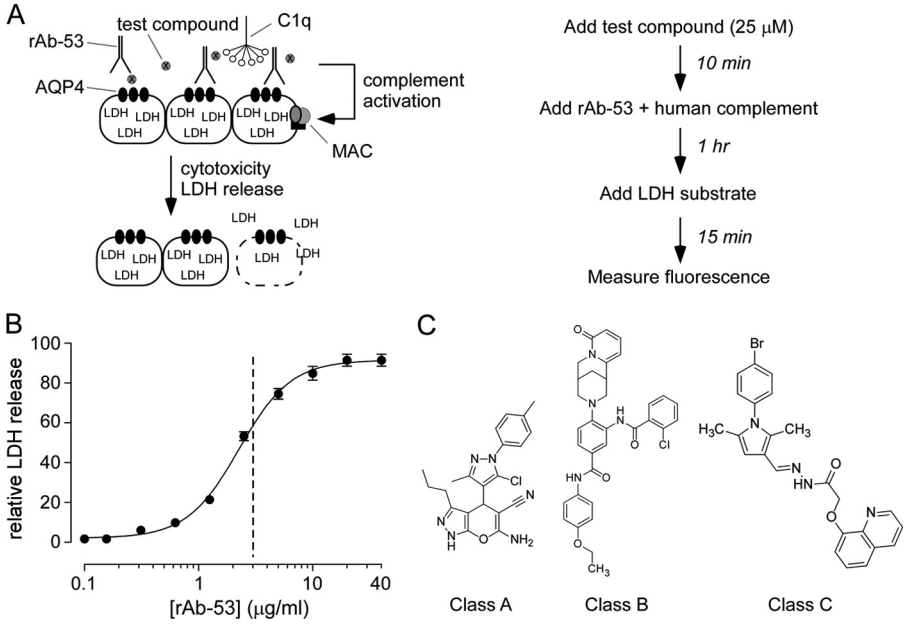

FIGURE 1. **High-throughput screen for identification of inhibitors of NMO-rAb/complement-mediated cytotoxicity.** *A*, *left*, schematic of the screening assay, which measures LDH release from M23-AQP4-expressing CHO cells treated with NMO recombinant monoclonal antibody rAb-53 and 2% complement. *Right*, flow diagram of the screening assay. *B*, dependence of complement-dependent cytotoxicity on rAb-53 concentration in CHO cells in the presence of 2% complement (S.E., $n = 4$). The *dashed vertical line* indicates rAb-53 concentration used for screening. *C*, chemical structures of three classes of inhibitors identified from screening. *MAC*, membrane attack complex.

of immunoglobulin structure) was used to create a structural model for the rAb-53 antigen-binding domain (20). Truncated sequences of the rAb-53 light chain (residues 1–117) and heavy chain (residues 118–249) were identified based on alignment with conserved Fab sequences. Complementarity-determining regions (CDRs) are indicated (underlined) in the truncated light chain sequence (EIVLTQSPGTLSLSPGERATLSCRASQTVRTNYLAWFQQKPGQAPRLLIFGASSRATGIPDRFSGSGSGTDFTLTISRLEPEDFAVYYCQQYGSSPWTFGQGTKVEIKRT; CDR-L1, CDR-L2, and CDR-L3) and heavy chain sequence (QVQLQESGAGLVKPSETLSLTCTVSGGSISGHYWNWIRQPPGKGLEWIGYIHYSGSTNYNPSLKSRVTISVDTSKNQFSLKLSSVTAADTAVYYCARAEGRGWSAFYYYYMEVWGKGSTVSVS; CDR-H1, CDR-H2, and CDR-H3). PIGS identified a template based on a structure of a Fab fragment of human IgM cold agglutinin (Protein Data Bank code 1DN0) with 90.1% sequence homology to the rAb-53 light chain and 72.6% homology to the heavy chain. Side chain conformations were modeled using SCWRL 3.0 (21). The rAb-53 structure was prepared for docking using the FRED_RECEPTOR utility (OpenEye Scientific Software). Initial docking computations were done using the rAb-53 Fab structure to identify potential small molecule-binding sites on the antibody surface. The ligand structures for A-01 and A-72 (two enantiomers for each) were prepared using a protocol in SciTegic Pipeline Pilot (Accelrys) to generate the proper ionization state at pH 7.4, and the molecules were then converted into energy-minimized three-dimensional structures. The ligand structures were passed through OMEGA v2.4.6 (OpenEye Scientific Software) to generate conformational libraries, which were subsequently assigned MMFF partial charges using MOLCHARGE v1.5.0 (OpenEye Scientific Software). The ligand structures were docked into the rAb-53 receptor model using FRED v.2.2.5 (OpenEye Scientific Software), free of pharmacophore restraint, and configured to employ consensus docking with its full suite of seven scoring functions. Partial charges were assigned to the rAb-53 receptor using the MMFF model with FRED prior to ligand docking. The final protein-ligand complexes were visualized using PyMOL (Schrödinger LLC, San Diego, CA).

RESULTS

Small-molecule Screen—A high-throughput screen was implemented to identify small-molecule inhibitors of complement-dependent cytotoxicity caused by a human NMO monoclonal autoantibody, rAb-53, which was characterized previously (12, 17). Binding of complement protein C1q to rAb-53 initiates the classical complement activation pathway (Fig. 1*A*). Cytotoxicity was measured by LDH release in CHO cells stably expressing the M23 isoform of human AQP4. As diagrammed in Fig. 1*A*, the screen involved addition of rAb-53 and human complement in the presence of test compound, a 60-min incubation, and enzymatic assay of LDH release. Maximum LDH release (100% cytotoxicity) was determined by treatment of cells with 0.1% Triton X-100. Fig. 1*B* shows LDH release as a function of rAb-53 concentration at fixed 2% complement. A rAb-53 concentration of 3 μg/ml (*dashed vertical line*) was used for screening. The screen was robust, with a statistical Z'-factor generally >0.6.

Screening of 50,000 small molecules gave 33 compounds that inhibited LDH release by >50% at 25 μM. Secondary screening indicated many of the active compounds to be false positives, as they inhibited components of the LDH enzymatic assay. The chemical structures of three verified classes of compounds with the greatest potency are shown in Fig. 1*C*. Further analysis of the pyrano[2,3-*c*]pyrazole class of compounds (Class A) was

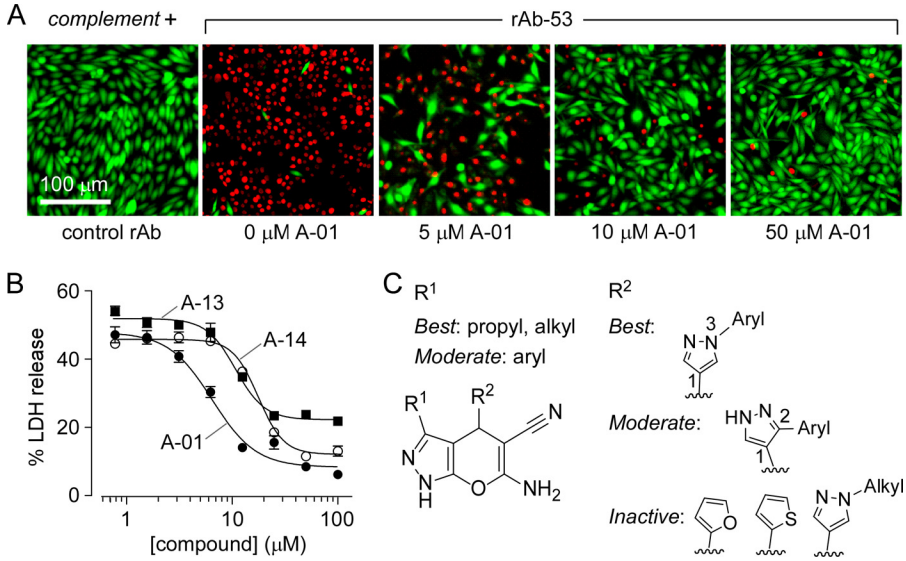

FIGURE 2. **Small-molecule blocker inhibits rAb-53- and complement-dependent cytotoxicity.** *A*, fluorescence micrographs showing live/dead (*green*/*red*) staining of AQP4-expressing CHO cells after 1 h of incubation at room temperature with 3 μg/ml rAb-53 and 2% complement in the presence of the indicated concentrations of inhibitor A-01. *B*, concentration dependence of LDH release as a function of inhibitor concentration after 1 h of incubation at room temperature with 3 μg/ml rAb-53 and 2% complement. *C*, structural determinants of inhibitor activity.

performed because of its interesting, idiotype-specific blocking mechanism (see below).

Structure-Activity Analysis of Pyrano[2,3-c]pyrazoles—Fig. 2*A* shows a live/dead cytotoxicity assay in which AQP4-expressing CHO cells were exposed to rAb-53 and 2% human complement in the presence of the indicated concentrations of A-01 and then stained to reveal live cells as green and dead cells as red. Compound A-01 reduced cytotoxicity in a concentration-dependent manner. Eighty-two commercially available pyrano[2,3-*c*]pyrazoles were tested. Fig. 2*B* shows the concentration dependence of LDH release for the most potent inhibitor, A-01, and for two other active analogs. Six compounds showed activity with IC_{50} values from 6.6 to 32 μM (Table 1). Fig. 2*C* summarizes the structural determinants of activity, which revealed that pyrano[2,3-*c*]pyrazoles bearing a single ring at the R^2 position were inactive. Active analogs contained two rings, with compounds having 1,3-linkage between the rings being more potent than those with 1,2-linkage (*e.g.* A-01 *versus* A-48). For the R^1 substituent, small linear alkyl groups and substituted phenyls were tolerated, although a bulky alkyl group reduced activity (*e.g.* A-01 *versus* A-14).

Pyrano[2,3-c]pyrazole A-01 Reduces NMO Pathology in the Spinal Cord Slice Culture Model—A clinically important consequence of NMO-IgG-dependent cytotoxicity in the central nervous system is the development of lesions with loss of AQP4 and GFAP immunoreactivity, as well as inflammation and demyelination. We previously developed an *ex vivo* model of NMO that recapitulates the major *in vivo* findings of NMO (19). As diagrammed in Fig. 3*A*, 300-μm-thick spinal cord slices were cultured for 7 days; incubated for 24 h with NMO-IgG, complement, and/or blocker; and then immunostained for AQP4 and GFAP as markers of NMO pathology. Fig. 3*B* shows a marked loss of AQP4 and GFAP immunoreactivity in spinal cord slices incubated for 24 h with 10 μg/ml rAb-53 and 5% complement. Fig. 3*C* summarizes lesion scores (0, no pathology; and 4, extensive pathology). Inclusion of A-01 during the

TABLE 1
Inhibition activity of pyrano[2,3-*c*]pyrazoles

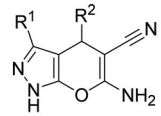

Compound	R^1	R^2	IC_{50} (μM)
A-01		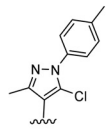	6.6
A-13		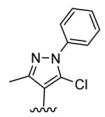	11
A-14		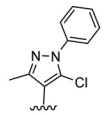	16
A-48	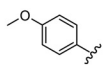	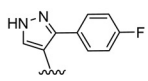	22
A-52	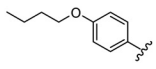	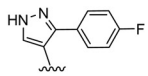	32
A-63	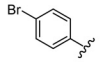	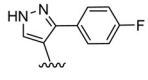	30

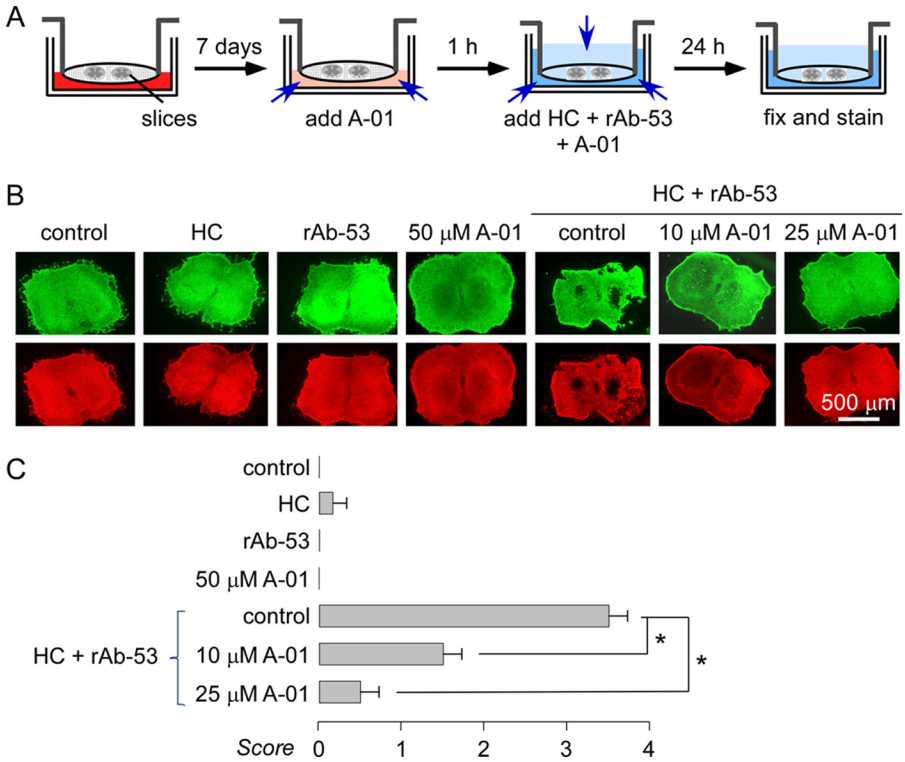

FIGURE 3. **Inhibitor A-01 reduces pathology in an *ex vivo* spinal cord slice model of NMO.** *A*, schematic of the spinal cord slice model of NMO. Mouse spinal cord slices were cultured for 7 days, followed by 24 h in the presence of antibody rAb-53 (10 μg/ml) and/or human complement (*HC*; 5%) without or with A-01 (10 and 25 μM). *B*, immunofluorescence of AQP4 (*red*) and GFAP (*green*). *C*, NMO lesion scores (S.E., $n = 4-6$). *, $p < 0.01$.

24-h incubation with rAb-53 and complement significantly reduced lesion severity in a concentration-dependent manner. In control studies, rAb-53 or complement alone did not produce pathology, nor did A-01 alone.

Idiotype Specificity of Pyrano[2,3-c]pyrazoles—To determine whether the pyrano[2,3-*c*]pyrazoles target rAb-53 or AQP4, binding and cytotoxicity were measured with other NMO monoclonal antibodies and with NMO polyclonal antibodies in NMO patient sera. Fig. 4*A* shows a binding assay in which AQP4-expressing cells were incubated with NMO-rAb and then a red fluorescent anti-human secondary antibody; AQP4 was immunostained green. Whereas rAb-53 binding was reduced by A-01, the binding of a different NMO recombinant antibody, rAb-58 (as characterized previously (17)), was not affected. Fig. 4*B* summarizes the A-01 concentration dependence data for rAb-53 and rAb-58 binding to AQP4 using an HRP-based Amplex Red fluorescence assay. Binding of rAb-53 to AQP4 was reduced by up to 75%, whereas binding of rAb-58 was not affected.

Fig. 4*C* summarizes the complement-dependent cytotoxicity for several NMO monoclonal antibodies and human NMO sera. Although A-01 greatly reduced cytotoxicity produced by rAb-53, it did not protect for the other monoclonal antibodies or for NMO patient sera, including the serum of the patient (serum 4) from which rAb-53 was isolated. The lack of cytoprotection for serum 4 indicates that rAb-53 is a minor component of total NMO-IgG.

SPR Shows Specific rAb-53 Binding—The rAb idiotype specificity data above suggest that A-01 targets rAb-53 rather than AQP4. SPR was done to investigate A-01 binding to rAb-53. For SPR measurements, rAb-53, rAb-58, and control antibody rAb-2B4 were covalently immobilized by standard primary amine coupling to the carboxymethylated dextran matrix of a CM5 sensor chip. Fig. 5*A* shows binding curves for A-01 with rAb-53, rAb-58, and rAb-2B4. A-01 produced a concentration-dependent increase in the SPR signal for rAb-53, showing characteristic fast binding and dissociation for small molecule-protein interactions. A-01 showed no binding to rAb-58 or rAb-2B4. Used as another control, an inactive pyrano[2,3-*c*]pyrazole analog, A-72, showed no binding interaction with rAb-53 (Fig. 5*B*). The dissociation constant (K_d) for A-01 binding to rAb-53 was estimated as 51 $\pm$ 20 μM (Fig. 5*C*).

Computational Analysis of the Pyrano[2,3-c]pyrazole-binding Site on rAb-53—Fig. 6*A* shows the relatively large size of rAb-53 compared with AQP4, which is assembled in membranes as tetramers that form higher order aggregates. Antibody modeling and molecular docking computations, as described under "Experimental Procedures," indicated a putative binding site for A-01 in the vicinity of the highly variable CDR-H3 and CDR-L2 regions. Docking was also done for the inactive analog A-72 (see Fig. 5*B*). Because A-01 and A-72 each possess a single chiral center, both enantiomers of A-01 and A-72 were examined individually. Both enantiomers of A-01 showed significantly improved docking scores compared with A-72 using consensus scoring across seven independent scoring functions implemented in the docking software (consensus scores of 6–7 *versus* 14–15 for A-01 and A-72, respectively). Close examination of the docking pose of A-01 (*R*-enantiomer) shows that both the lipophilic propyl and *para*-methylphenyl groups make significant complementary hydrophobic contacts with the rAb-53 rAb surface (Fig. 6*B*).

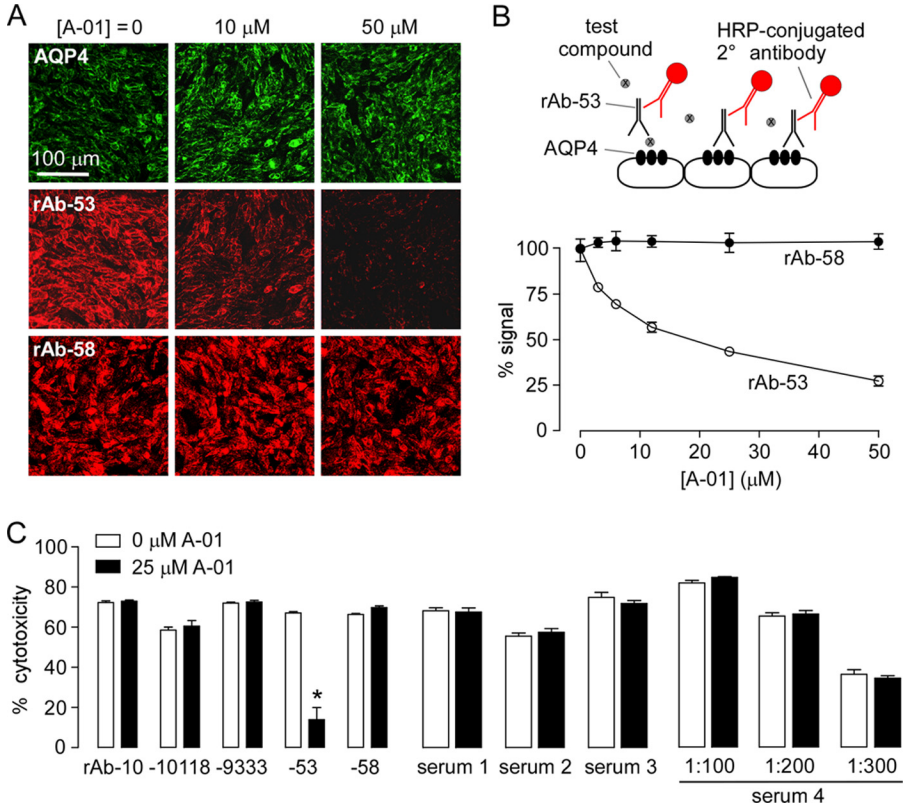

FIGURE 4. **Idiotype specificity for A-01 inhibition of rAb-53 binding to AQP4 and complement-dependent cytotoxicity.** *A*, binding of NMO monoclonal antibodies rAb-53 and rAb-58 (*red*), shown with AQP4 immunofluorescence (*green*) in M23-AQP4-expressing CHO cells. Cells were incubated with the indicated concentrations of A-01 for 30 min before addition of NMO antibody (1 μg/ml) and anti-AQP4 antibody (0.4 μg/ml). *B*, *upper*, schematic of HRP fluorescence assay. *Lower*, A-01 concentration-dependent inhibition of binding of rAb-53 and rAb-58 (1 μg/ml each) to AQP4 (S.E., $n = 4$). *C*, complement-dependent cytotoxicity measured for the indicated NMO-rAbs (*left*), NMO patient sera (*center*), and the serum of the patient in which rAb-53 was identified (*right*; tested at three dilutions) (S.E., $n = 4$). *, $p < 0.001$.

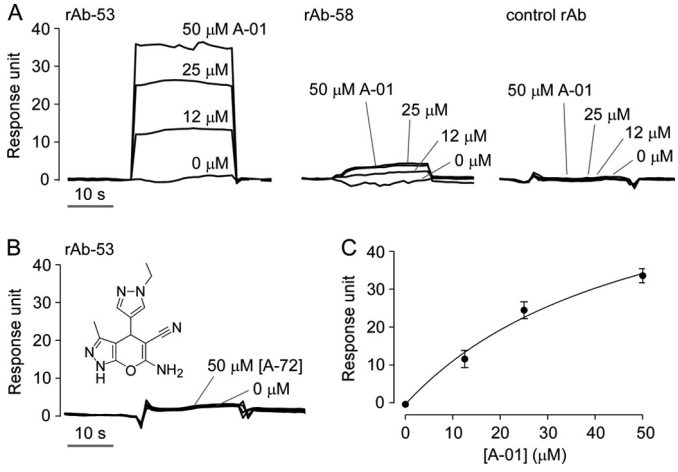

FIGURE 5. **A-01 binding to rAb-53 measured by SPR.** *A*, sensorgram showing concentration-dependent binding of A-01 to rAb-53 (*left*) but not to rAb-58 (*center*) or rAb-2B4 (*right*). Antibodies were ligated onto a CM5 sensor chip using standard primary amine coupling chemistry. A-01 was injected for 25 s over the antibodies at a flow rate of 30 μl/min. *B*, control study showing that the inactive analog A-72 did not bind to rAb-53. *C*, binding affinity of A-01 for rAb-53 ($K_d = 51 \pm 20$ μM).

DISCUSSION

A cytotoxicity-based small-molecule screen yielded blockers of the binding of a human NMO monoclonal autoantibody to its cell surface target, AQP4. We previously reported small-molecule and antibody blockers of NMO-IgG binding to AQP4 that targeted the extracellular surface of AQP4 and blocked the binding of polyclonal NMO-IgG to AQP4 and downstream cytotoxicity (12, 13). Here, we identified a class of small molecules that exclusively blocked AQP4 binding of the NMO monoclonal antibody used for screening. The compounds did not interfere with AQP4 binding of other monoclonal or polyclonal (from NMO patient sera) NMO-IgG and were found to bind directly to the monoclonal antibody used for screening. We conclude that the pyrano[2,3-*c*]pyrazoles identified here are idiotype-specific for rAb-53, demonstrating for the first time, to our knowledge, the development of idiotype-specific small-molecule blockers.

The NMO monoclonal antibody used here, rAb-53, is a recombinant monoclonal antibody of IgG1 isotype that was generated from sequence analysis of a clonally expanded plasmablast population in the cerebrospinal fluid of an NMO patient (15). The rAb contains an antigen-binding site composed of a VH4–59 heavy chain and a VK3 light chain. Fluorescence cell binding assays gave a dissociation constant of 44 nM for binding of rAb-53 to AQP4 (17). Slow dissociation of rAb-53 from AQP4 over many hours was found in unbinding assays in live cells and SPR measurements in AQP4-reconstituted proteoliposomes (13). The Fc portion of rAb-53 has been mutated to generate aquaporumab blocking antibodies that lack effector functions (13). The target of rAb-53 binding, AQP4, functions as a water-selective channel in astrocytes,

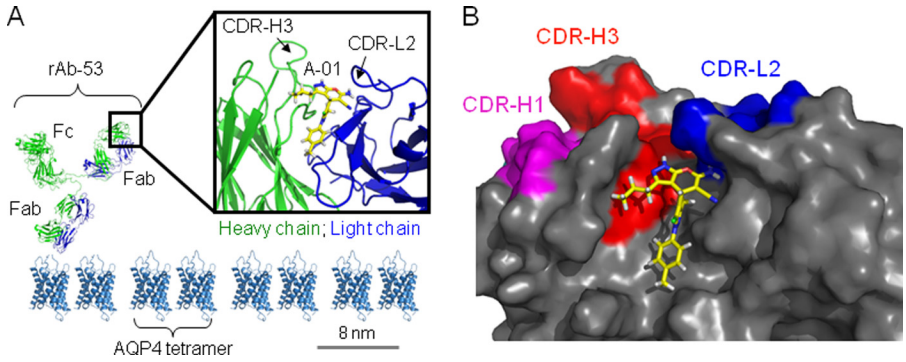

FIGURE 6. **Putative binding site of A-01 on rAb-53.** *A*, zoomed-out view of rAb-53 showing A-01 (*R*-enantiomer) binding as determined by docking computations. The structure and size of AQP4 (Protein Data Bank code 3GD8) are shown for comparison. *B*, zoomed-in view of A-01 docked onto the surface of rAb-53 showing proximity to the CDR-H3 and CDR-L2 regions.

where it is involved in a variety of biological functions, including brain water balance, neuroexcitation, astrocyte migration, glial scarring, and neuroinflammation (22). AQP4 monomers of ~30 kDa assemble at the cell plasma membrane as tetramers that form supramolecular aggregates called orthogonal arrays of particles (23, 24). The affinity of rAb-53 binding to AQP4 arrays is ~5-fold higher than that to individual AQP4 tetramers (17). NMO patient serum consists of a polyclonal mixture of autoantibodies that bind to various three-dimensional epitopes on the AQP4 extracellular surface. The inability of A-01 to prevent binding of serum NMO-IgG of the patient from which rAb-53 was isolated indicates that rAb-53 is, at most, a minor component in that patient serum.

Pyrano[2,3-*c*]pyrazoles, as identified here, are reported to have a broad range of biological activities. A pyrano[2,3-*c*]pyrazole was found to bind to Bcl-2 protein and induce apoptosis in human acute myeloid leukemia cells with EC_{50} ~18 μM (25). Virtual screening against the ATP-binding site of Chk1 kinase identified a pyrano[2,3-*c*]pyrazole as an inhibitor with IC_{50} ~20 μM (26). Certain pyrano[2,3-*c*]pyrazoles were reported to exhibit molluscicidal activity toward *Biomphalaria alexandrina* snails at low nanomolar concentration (27). Another study reported anti-inflammatory effects of pyrano[2,3-*c*]pyrazoles in carrageenan-challenged rats in which high (>500 mg/kg) oral doses were tolerated without apparent toxicity (28). As pyrano[2,3-*c*]pyrazoles contain one chiral center, a pure enantiomer of A-01 is likely to have greater inhibition potency compared with the racemic mixture studied here. Synthetically, racemic pyrano[2,3-*c*]pyrazoles are prepared via a four-component, one-pot reaction (29). The molecular docking studies here showed a putative binding site for pyrano[2,3-*c*]pyrazoles on rAb-53 near the highly variable CDR-L2 and CDR-H3 regions. Preparation of a computationally designed focused library of analogs might produce compounds with nanomolar potency.

Idiotype-specific small molecules have potential applications as research tools and as therapeutics. Small-molecule blockers of antibody-target interactions could be used to modulate or terminate the action of an administered monoclonal antibody therapeutic. For example, natalizumab is a humanized IgG4 recombinant monoclonal antibody that binds the α4 subunit of the $\alpha4\beta1$ integrin and is highly effective for the treatment of relapsing forms of multiple sclerosis. However, natalizumab therapy is complicated by the risk of a potentially lethal infection with the human polyoma JC virus, progressive multifocal leukoencephalopathy (30). Although progressive multifocal leukoencephalopathy is untreatable, an important initial step in management of natalizumab induction of this infection is rapid depletion of circulating antibody with plasma exchange (31). Early treatment with an idiotype-specific small-molecule blocker of natalizumab could displace bound antibody, restore T cell migration, and expedite immune reconstitution.

As another example, IgM, IgG, or IgA monoclonal gammopathies may be found in B cell lymphoproliferative disorders (Waldenström macroglobulinemia, B cell lymphoma, multiple myeloma) or in normal individuals (monoclonal gammopathy of undetermined significance). Some individuals with monoclonal gammopathies have neuropathic syndromes driven by antibody binding to protein or ganglioside components of peripheral nerve myelin (32). In these disorders, treatment of the underlying malignancy may be augmented by anti-idiotype therapy to remove pathogenic antibody from its peripheral nerve target. Similarly, in rare paraneoplastic disorders such as NMDA encephalitis (33), idiotype-selective small-molecule therapy may dissociate pathogenic antibody from its CNS target and reduce seizure activity.

In conclusion, a cytotoxicity-based small-molecule screen identified pyrano[2,3-*c*]pyrazoles as idiotype-specific inhibitors of binding of a human NMO monoclonal antibody to the astrocyte water channel AQP4. Idiotype-specific small molecules have potential as therapeutics for diseases that are caused by binding of pathogenic monoclonal antibodies to their target antigen, such as natalizumab-induced multifocal leukoencephalopathy and certain monoclonal gammopathies and paraneoplastic disorders. The identification of idiotype-specific pyrano[2,3-*c*]pyrazoles provides proof of concept for an antibody-targeted small-molecule blocker strategy to prevent specific antibody-antigen binding.

REFERENCES

1. Chan, A. C., and Carter, P. J. (2010) Therapeutic antibodies for autoimmunity and inflammation. *Nat. Rev. Immunol.* **10,** 301–316
2. Nelson, A. L., Dhimolea, E., and Reichert, J. M. (2010) Development trends for human monoclonal antibody therapeutics. *Nat. Rev. Drug Discov.* **9,** 767–774
3. Vincent, A., Bein, C. G., Irani, S. R., and Waters, P. (2011) Autoantibodies associated with diseases of the CNS: new developments and future chal-

lenge. *Lancet Neurol.* **10,** 759–772
4. Cree, B. (2008) Neuromyelitis optica: diagnosis, pathogenesis, and treatment. *Curr. Neurol. Neurosci. Rep.* **8,** 427–433
5. Jarius, S., and Wildemann, B. (2010) AQP4 antibodies in neuromyelitis optica: diagnostic and pathogenetic relevance. *Nat. Rev. Neurol.* **6,** 383–392
6. Papadopoulos, M. C., and Verkman, A. S. (2012) Aquaporin-4 and neuromyelitis optica. *Lancet Neurol.* **11,** 535–544
7. Nielsen, S., Nagelhus, E. A., Amiry-Moghaddam, M., Bourque, C., Agre, P., and Ottersen, O. P. (1997) Specialized membrane domains for water transport in glial cells: high-resolution immunogold cytochemistry of aquaporin-4 in rat brain. *J. Neurosci.* **17,** 171–180
8. Hinson, S. R., Pittock, S. J., Lucchinetti, C. F., Roemer, S. F., Fryer, J. P., Kryzer, T. J., and Lennon, V. A. (2007) Pathogenic potential of IgG binding to water channel extracellular domain in neuromyelitis optica. *Neurology* **69,** 2221–2231
9. Marignier, R., Nicolle, A., Watrin, C., Touret, M., Cavagna, S., Varrin-Doyer, M., Cavillon, G., Rogemond, V., Confavreux, C., Honnorat, J., and Giraudon, P. (2010) Oligodendrocytes are damaged by neuromyelitis optica immunoglobulin G via astrocyte injury. *Brain* **133,** 2578–2591
10. Parratt, J. D., and Prineas, J. W. (2010) Neuromyelitis optica: a demyelinating disease characterized by acute destruction and regeneration of perivascular astrocytes. *Mult. Scler.* **16,** 1156–1172
11. Saadoun S., Waters P., Bell B. A., Vincent A., Verkman A. S., and Papadopoulos M. C. (2010) Intracerebral injection of neuromyelitis optica immunoglobulin G and human complement produces neuromyelitis optica lesions in mice. *Brain* **133,** 349–361
12. Tradtrantip, L., Zhang, H., Anderson, M. O., Saadoun, S., Phuan, P. W., Papadopoulos, M. C., Bennett, J. L., and Verkman, A. S. (2012) Small-molecule inhibitors of NMO-IgG binding to aquaporin-4 reduce astrocyte cytotoxicity in neuromyelitis optica. *FASEB J.* **26,** 2197–2208
13. Tradtrantip, L., Zhang, H., Saadoun, S., Phuan, P. W., Lam, C., Papadopoulos, M. C., Bennett, J. L., and Verkman, A. S. (2012) Anti-aquaporin-4 monoclonal antibody blocker therapy for neuromyelitis optica. *Ann. Neurol.* **71,** 314–322
14. Phuan, P. W., Ratelade, J., Rossi, A., Tradtrantip, L., and Verkman, A. S. (2012) Complement-dependent cytotoxicity in neuromyelitis optica requires aquaporin-4 protein assembly in orthogonal arrays. *J. Biol. Chem.* **287,** 13829–13839
15. Bennett, J. L., Lam, C., Kalluri, S. R., Saikali, P., Bautista, K., Dupree, C., Glogowska, M., Case, D., Antel, J. P., Owens, G. P., Gilden, D., Nessler, S., Stadelmann, C., and Hemmer, B. (2009) Intrathecal pathogenic anti-aquaporin-4 antibodies in early neuromyelitis optica. *Ann. Neurol.* **66,** 617–629
16. Wingerchuk, D. M., Lennon, V. A., Pittock, S. J., Lucchinetti, C. F., and Weinshenker, B. G. (2006) Revised diagnostic criteria for neuromyelitis optica. *Neurology* **66,** 1485–1489
17. Crane, J. M., Lam, C., Rossi, A., Gupta, T., Bennett, J. L., and Verkman, A. S. (2011) Binding affinity and specificity of neuromyelitis optica autoantibodies to aquaporin-4 M1/M23 isoforms and orthogonal arrays. *J. Biol. Chem.* **286,** 16516–16524
18. Ma, T., Yang, B., Gillespie, A., Carlson, E. J., Epstein, C. J., and Verkman, A. S. (1997) Generation and phenotype of a transgenic knockout mouse lacking the mercurial-insensitive water channel aquaporin-4. *J. Clin. Invest.* **100,** 957–962
19. Zhang, H., Bennett, J. L., and Verkman, A. S. (2011) *Ex vivo* spinal cord slice model of neuromyelitis optica reveals novel immunopathogenic mechanisms. *Ann. Neurol.* **70,** 943–954
20. Marcatili, P., Rosi, A., and Tramontano, A. (2008) PIGS: automatic prediction of antibody structures. *Bioinformatics* **24,** 1953–1954
21. Wang, Q., Canutescu, A. A., and Dunbrack, R. L., Jr. (2008) SCWRL and MolIDE: computer programs for side chain conformation prediction and homology modeling. *Nat. Protoc.* **3,** 1832–1847
22. Verkman, A. S. (2011) Aquaporins at a glance. *J. Cell Sci.* **124,** 2107–2112
23. Yang, B., Brown, D., and Verkman, A. S. (1996) The mercurial-insensitive water channel (AQP4) forms orthogonal arrays in stably transfected Chinese hamster ovary cells. *J. Biol. Chem.* **271,** 4577–4580
24. Verbavatz, J. M., Ma, T., Gobin, R., and Verkman, A. S. (1997) Absence of orthogonal arrays in kidney, brain, and muscle from transgenic knockout mice lacking water channel aquaporin-4. *J. Cell Sci.* **110,** 2855–2860
25. Wang, J. L., Liu, D., Zhang, Z. J., Shan, S., Han, X., Srinivasula, S. M., Croce, C. M., Alnemri, E. S., and Huang, Z. (2000) Structure-based discovery of an organic compound that binds Bcl-2 protein and induces apoptosis of tumor cells. *Proc. Natl. Acad. Sci. U.S.A.* **97,** 7124–7129
26. Foloppe, N., Fisher, L. M., Howes, R., Potter, A., Robertson, A. G., and Surgenor, A. E. (2006) Identification of chemically diverse Chk1 inhibitors by receptor-based virtual screening. *Bioorg. Med. Chem.* **14,** 4792–4802
27. Abdelrazek, F. M., Metz, P., Metwally, N. H., and El-Mahrouky, S. F. (2006) Synthesis and molluscicidal activity of new cinnoline and pyrano[2,3-*c*]pyrazole derivatives. *Arch. Pharm.* **339,** 456–460
28. Zaki, M. E.., Soliman, H. A., Hiekal, O. A., and Rashad, A. E. (2006) Pyrazolopyranopyrimidines as a class of anti-inflammatory agents. *Z. Naturforsch. C* **61,** 1–5
29. Litvinov, Y. M., Shestopalov, A. A., Rodinovskaya, L. A., and Shestopalov, A. M. (2009) New convenient four-component synthesis of 6-amino-2,4-dihydropyrano[2,3-*c*]pyrazol-5-carbonitriles and one-pot synthesis of 6′-aminospiro[(3*H*)-indol-3,4′-pyrano[2,3-*c*]pyrazol]-(1*H*)-2-on-5′-carbonitriles. *J. Comb. Chem.* **11,** 914–919
30. Kleinschmidt-DeMasters, B. K., and Tyler, K. L. (2005) Progressive multifocal leukoencephalopathy complicating treatment with natalizumab and interferon β1a for multiple sclerosis. *N. Engl. J. Med.* **353,** 369–374
31. Khatri, B. O., Man, S., Giovannoni, G., Koo, A. P., Lee, J. C., Tucky, B., Lynn, F., Jurgensen, S., Woodworth, J., Goelz, S., Duda, P. W., Panzara, M. A., Ransohoff, R. M., and Fox, R. J. (2009) Effect of plasma exchange in accelerating natalizumab clearance and restoring leukocyte function. *Neurology* **72,** 402–429
32. Lozeron, P., and Adams, D. (2007) Monoclonal gammopathy and neuropathy. *Curr. Opin. Neurol.* **20,** 536–541
33. Irani, S. R., and Vincent, A. (2011) NMDA receptor antibody encephalitis. *Curr. Neurol. Neurosci. Rep.* **11,** 298–304